Available online at www.sciencedirect.com
SCIENCE DIRECT
Journal of the European Ceramic Society 26 (2006) 1725–1736
www.elsevier.com/locate/jeurceramsoc

The yttria-stabilized zirconia and interfacial coating on Nicalon™ fiber

N.I. Baklanova [a,*], A.T. Titov [b], A.I. Boronin [c], S.V. Kosheev [c]

[a] *Institute of Solid State Chemistry and Mechanochemistry, SB RAS, Kutateladze St. 18, Novosibirsk 630128, Russian Federation*
[b] *General Institute of Geology, Geophysics and Mineralogy, SB RAS, Novosibirsk 630090, Russian Federation*
[c] *Boreskov Institute of Catalysis, SB RAS, Novosibirsk 630090, Russian Federation*

Received 15 November 2004; received in revised form 24 February 2005; accepted 5 March 2005
Available online 3 May 2005

Abstract

Sols of yttria-stabilized zirconia may be used as simple, readily processable and accurate controllable precursors for the ZrO_2 interfacial coatings on SiC-based Nicalon™ fibers. The ZrO_2 interfacial coatings of predictable crystal phase compositions were obtained in dependence of yttria dopant level. The morphology, composition and oxidation resistance of coated fibers were evaluated by SEM, EDS, XPS, XRD, and Raman analysis. All coatings obtained are uniform, continuous and adherent to substrates. The delamination within the ZrO_2 interfacial coating was found. Possible reasons of this phenomenon are discussed. The peculiarities of the behavior of Y-stabilized ZrO_2-coated fibers in air at elevated temperature are considered.

Keyword: Yttria-stabilized zirconia; Fibres; Interfaces; SiC; ZrO_2; Coatings

1. Introduction

Ceramic matrix composites (CMCs) reinforced by SiC-based fibers such as Nicalon™, Hi-Nicalon™, Sylramic® (SiC/SiC) achieve high toughness and damage tolerance through the disposal of weak fiber coating which can deflect cracks and promote debonding at the fiber/matrix region.[1] It is stated that conventional interphase materials, such as carbon and BN exhibit the environmental instability at operating temperatures.[2,3] Therefore, there is a strong interest to study alternative interfaces that would be more oxidation-resistant than carbon and BN coatings. Among alternative interphases the refractory oxide-based systems are considered as the most promising ones. [4–6]

The feasibility of using a CVD ZrO_2 fiber coating as an oxidation-resistant and weak interphase for SiC/SiC composites was thoroughly examined by Lee and coworkers[7–9] They found that the CVD ZrO_2 coating exhibited desired tensile failure behavior and extensive crack deflection within the interface region. They concluded that the delamination within ZrO_2 layer occurred as result of the martensitic transformation of t-ZrO_2 nuclei to m-ZrO_2 on reaching a critical grain size and the development of significant compressive hoop stresses due to volume dilation and shear associated with the martensitic transformation. The delamination to be observed for the ZrO_2 coating provides the retention of fiber strength. It should be noted that the delamination process can lead to breaking of the integrity of the fiber coating. It is undesirable feature considering the necessity of protection the fiber surface from matrix infiltration on following stages of the fabrication CMCs. Therefore, a dense undelaminated but compressively stressed coating might be preferred before infiltration. Thus, in order to optimize the interfacial properties of ZrO_2 as the fiber coating for SiC/SiC composites it is necessary accurately to control phase composition, morphology and an extent of phase transformation in the ZrO_2 coating layer.

Numerous studies demonstrated (see, e.g. review[10]), that an addition of Y_2O_3 or other oxides, such as CaO, MgO, CeO_2 results in an appearance of oxygen vacancies and the formation of the stabilized tetragonal phase of ZrO_2. The toughness of YSZ ceramics is strongly dependent on the volume fraction of tetragonal phase, with toughness de-

* Corresponding author. Tel.: +7 3832 363839; fax: +7 3832 322847.
E-mail address: baklanova@solid.nsc.ru (N.I. Baklanova).

0955-2219/$ – see front matter © 2005 Elsevier Ltd. All rights reserved.
doi:10.1016/j.jeurceramsoc.2005.03.241

creasing as a fraction of either the monoclinic or cubic phase increases. Besides, it was detected the relationships between the oxygen partial pressure and the nucleation and morphologic characteristics of the ZrO_2 coating that was formed by CVD or magnetron sputtering methods.[7–9,11] These relationships were attributed to the grain size and oxygen deficiency effects, which appear to cause the stabilization of t-ZrO_2. Thus, one can see that the ZrO_2 coating composed of predominantly tetragonal or cubic transformable phases can be fabricated with different experimental approaches.

Early we reported about the particularities of the formation of refractory oxide interfacial coatings including ZrO_2 coating on Nicalon™ fibers by sol–gel technique.[12] A mixture of the monoclinic and tetragonal modifications was detected in the ZrO_2 coating derived from sol–gel precursors, with the monoclinic being predominant. The columnar morphology was observed that could provide an easy, low-energy path for crack propagation. In order to either tough transformation or crack deflection mechanism to operate within interface zone the columnar morphology of ZrO_2 coating must be modified.

The aim of this work is to develop an approach to the formation of yttria-stablilized ZrO_2 interfacial coatings on Nicalon™ fiber and to study the peculiarities of their composition, morphology and oxidation resistance. For this purpose a sol–gel approach was chosen as main. The sol–gel process could be considered as one of the most convenient technique allowing us to produce the oxide interfacial coatings including zirconia coatings with controlled content of yttria and as a consequence with predictable phase composition and morphology.

2. Experimental

2.1. Substrate and coating preparation

Woven Nicalon™ NLM202 (Nippon Carbon Co. Japan) fiber cloths were used as substrate materials. Prior to coating, Nicalon™ fiber cloths were immersed for 24 h in 50:50 acetone–ethanol mixture for removing a sizing agent, after that they were dried at ambient temperature. Then they were thermally treated in air at 450 °C.

The coating process was based on the dipping of Nicalon™ fabrics into sols of hydrated oxide metals. Precursors for the Y_2O_3-partially-stabilized zirconia (Y-PSZ) coatings were the sols of hydrated yttrium–zirconium oxides with different ZrO_2:Y_2O_3 ratio. The preparation of initial sols was similar to that described by Yan and coworkers[13,14] The coating solution was prepared by dissolving yttrium nitrate hexahydrate $Y(NO_3)_3{\cdot}6H_2O$ and zirconyl chloride octahydrate $ZrOCl_2{\cdot}8H_2O$ (CG, the Hf content not more than 1%) at given molar ratio in appropriate amount of ethanol–water solution. The coating solution contained metal ion concentrations of 0.1 M. Sols with the 3 and 9 mol% Y_2O_3 content were prepared. Samples derived from these sols were named after the yttria content, i.e. 3Y-ZrO_2 means 3 mol% Y_2O_3 and 97 mol% ZrO_2. The coating stage involved firstly the immersion of the Nicalon™ fabrics into sols with different content of yttria. Then the specimens were dried on air at ambient temperature and then slowly heated till 960 °C in argon flow at atmospheric pressure. To increase of thickness of interfacial coating the dipping–annealing procedure was repeated several times.

Also the air-dried powders with different Y_2O_3 content were prepared using sol–gel approach to compare the properties of coatings and powders of the same composition.

2.2. Specimen characterization

The phases in sol–gel derived ZrO_2 and Y-PSZ powders and coatings were characterized by X-ray diffraction analysis (XRD) using monochromatic Cu Kα radiation with DRON-3 diffractometer (Russia). Scanning electron microscope SEM LEO 1430VP, supplied by EDX (Oxford) spectrometer was used for studying of morphology and composition of coated fibers.

The FT-Raman spectra of sol–gel derived ZrO_2 and Y-PSZ powders were recorded using a Bruker RFS 100/S spectrometer equipped with Nd-YAG laser operating at the 1064 nm excitation wavelength. The laser output was 100 mV. For each spectrum 100 scans were accumulated. Micro Raman spectra of the Y-PSZ-coated Nicalon™ fibers were recorded using a Triplemate, SPEX spectrometer equipped with CCD spectrometric detector and microscope attachment for back scattering geometry. The 488 nm radiation from an argon laser was used for spectral excitation.

XPS spectra were measured using VG ESCALAB spectrometer using Al Kα irradiation and calibrated against Au $4f_{7/2}$ ($E_b = 84.0$ eV) and Cu $2p_{3/2}$ ($E_b = 932.7$ eV) lines. Before measurements specimens were heated for 30 min at 600 °C in vacuum. All of spectra are represented in binding energy scale that was obtained with respect to C 1s peak of carbon at 284.8 eV. For spectroscopic analysis of electron spectra the original software CALC was applied to extract the detailed information about electron structure of coated fibers.

2.3. Oxidation tests

Thermal oxidation resistance of coated Nicalon™ fabrics was examined in air under static conditions at 1000 °C. The samples of Nicalon™ fabrics (100–200 mg) were placed in the preliminary heated furnace (KO-14, German) and kept during definite time intervals. Then the samples were taken out, cooled in dessicator and weighted with accuracy ± 0.1 mg. A total time of testing was 26 h.

3. Results

3.1. SEM/EDS analysis

SEM images of the undoped and Y-doped ZrO_2 coating on Nicalon™ fiber are represented in Fig. 1a–d. One can see

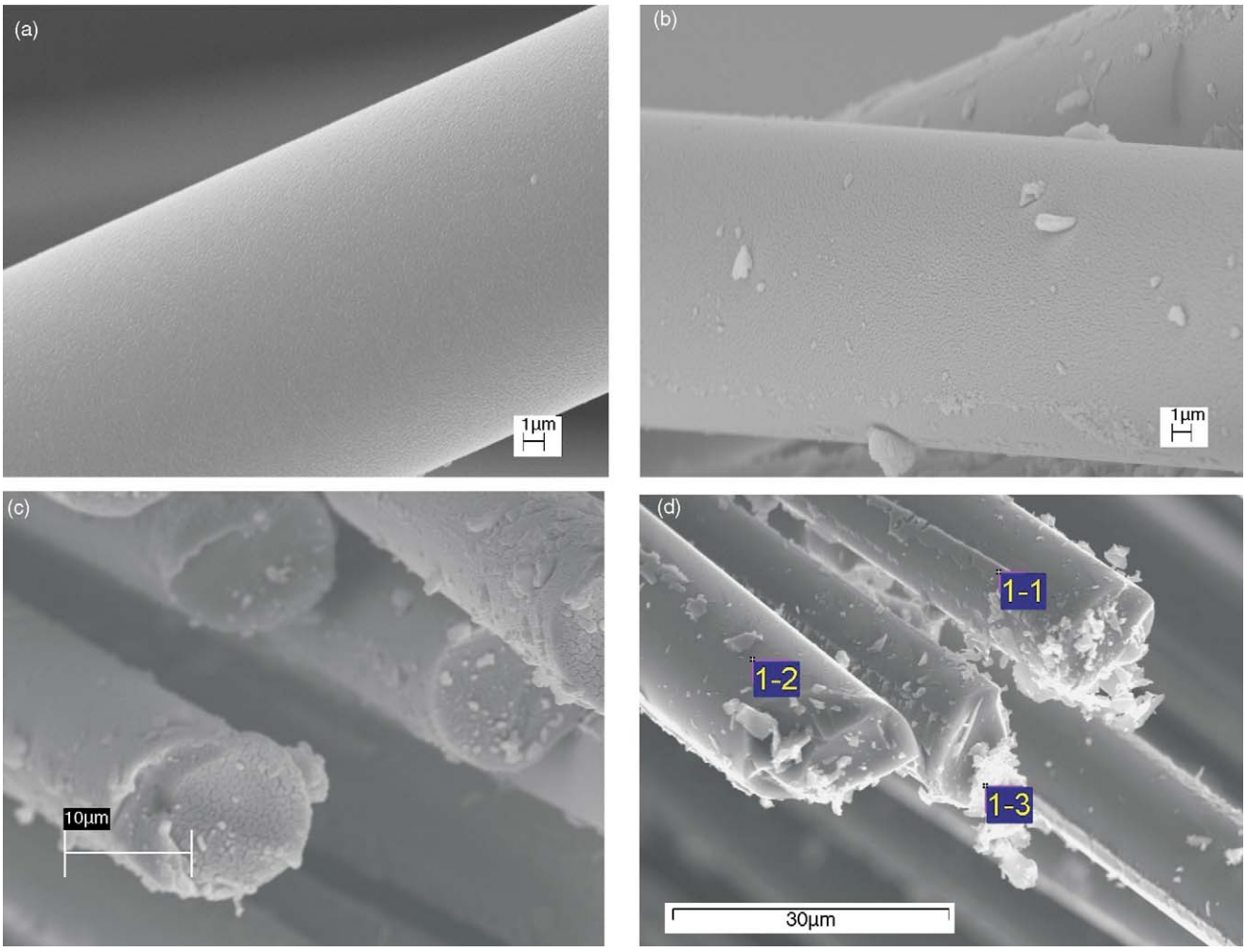

Fig. 1. (a–d) SEM images of the undoped (one cycle) and 9Y-ZrO_2 coating on Nicalon^{TM} fiber (two cycles).

(Fig. 1a), that the surface of undoped ZrO_2 coating is rather smooth and adherent to fiber. No fiber bridging, no spalling of coating was observed. The non-uniformities shaped as crystallized traces of coating sol that was retained between filaments within a tow bundle are seen on the surface of separate filaments. It should be noted that this is a rare occurrence. The thickness of coating after the first cycle, determined by SEM, is less than 80 nm.

A doping by yttrium (9Y-PSZ, two cycles) leads to significant change in the surface morphology (Fig. 1b). Separate well-developed crystals and aggregates of crystals can be observed at the edge of cross-section and the surface of each filament, especially on contacts of filaments in a bundle (Fig. 1c). Nevertheless, no bridging was observed (Fig. 1d). The thickness of coating evaluated from SEM image is about 300–400 nm. Upon a closer view one can see that the morphology of crystals is isometric unlike of columnar one that was observed for undoped ZrO_2 coating. The presence of Si, Zr, Y, O at areas which are marked in Fig. 1d is detected by EDS analysis (Fig. 2). In addition, the peaks belonging to other elements were detected in EDS spectra. They appear to originate from a contamination by glue and sample holder.

An increase of number of dipping–annealing till to 5 leads to strong nonuniformity of coating not only on length but cross-section of a filament too (Fig. 3a–d), the thickness being about 1 μm or more and variable at different filaments. A great number of large well-developed crystals and aggregates are observed on the surface of filaments. One could be proposed that nonuniformaties arising from the first cycles (see, e.g. Fig. 1b–d) could serve as centers of crystallization on the following steps of processing. Upon a closer view one can see that aggregates are consisted from nanosized (less than 100 nm) crystals (Fig. 3b). They have isometric round-shaped form. One can observe places where a delamination within coating occurs (Fig. 3c). A crack deflection phenomenon is distinctly detected at interfacial zone (Fig. 3d). Crack direction is changed from perpendicular to parallel to a fiber surface. This is accompanied by debonding at the coating/fiber interface.

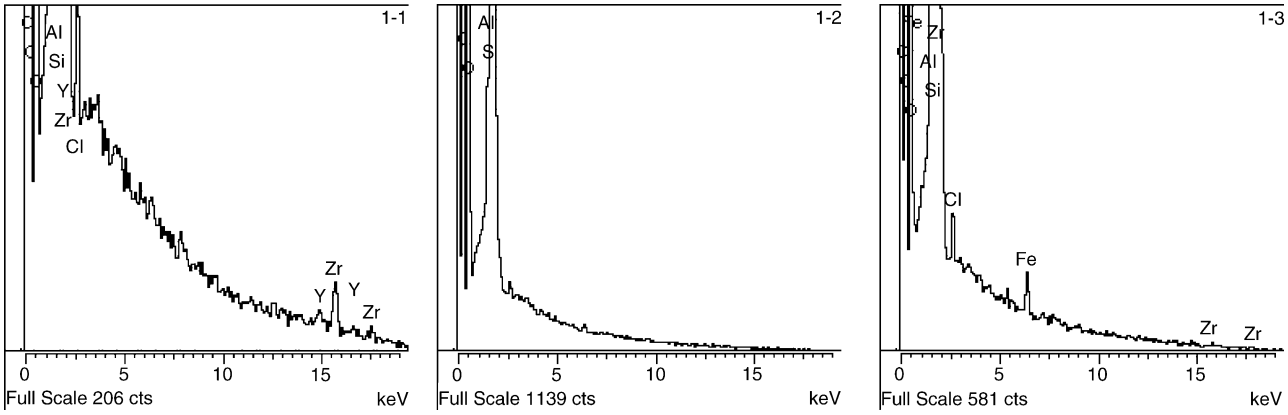

Fig. 2. EDS spectrum of the 9Y-ZrO_2 (two cycles) coating on Nicalon^{TM} fiber.

3.2. XPS analysis

Survey XPS spectrum recorded from the 9Y-PSZ (five cycles) coated Nicalon^{TM} fabrics revealed a presence of oxygen, silicon, carbon, zirconium, yttrium as main components (Fig. 4). After correction of intensities of C 1s, O 1s, Si 2p, Zr 3d and Y 3d lines for their atomic sensitivity factors (ASF) the elemental composition of surface layer can be evaluated.[15] The results are represented in Table 1. One can see from Fig. 4 that traces of sodium and nitrogen are present in coating. Nitrogen can be originated from the initial yttrium nitrate. Earlier, the traces of sodium were revealed by XPS analysis in initial Nicalon^{TM} fiber.[12] They could be introduced during processing of fiber or handling.

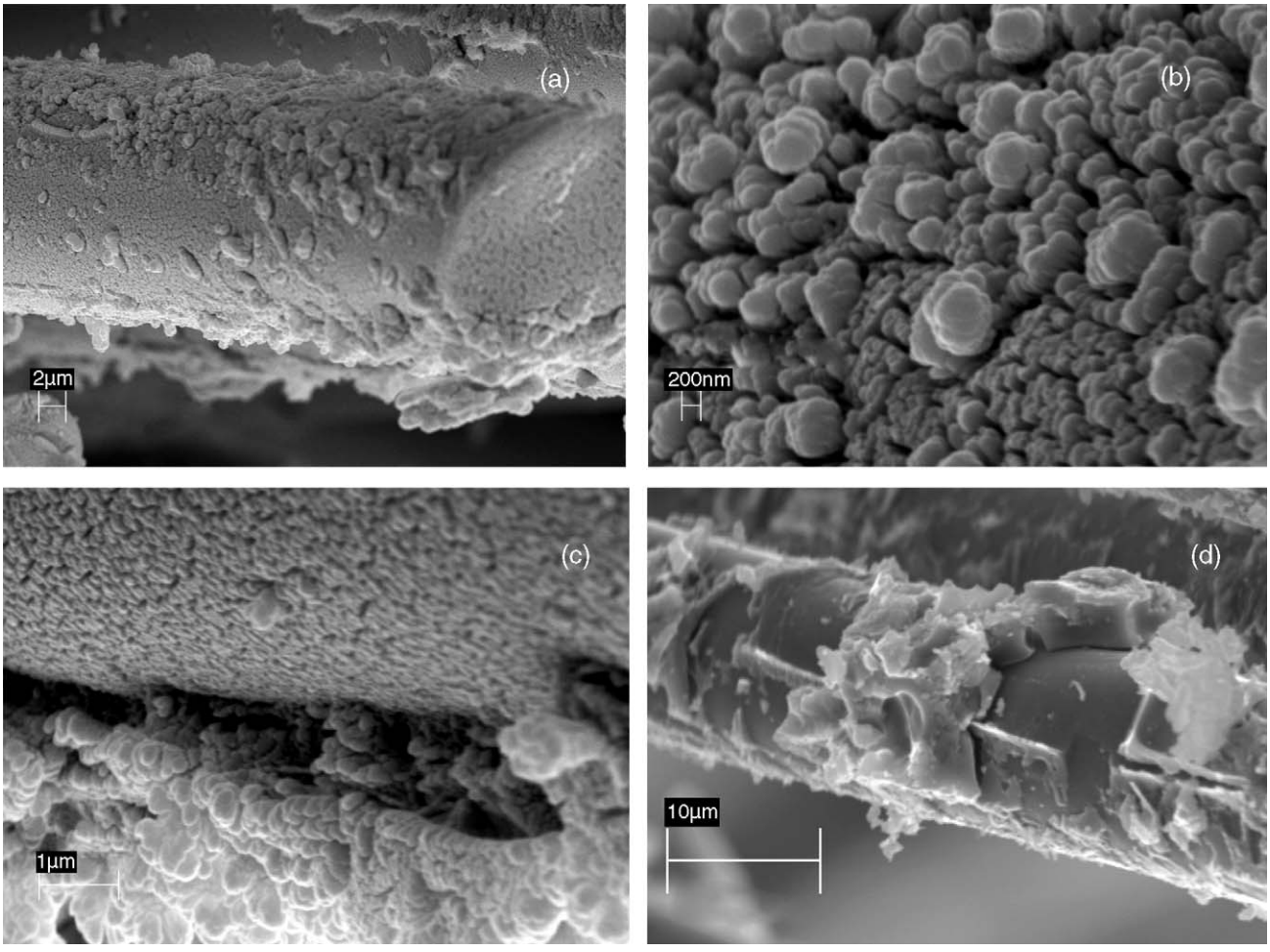

Fig. 3. (a–d) SEM images of the 9Y-ZrO_2 coating on Nicalon^{TM} fiber (five cycles).

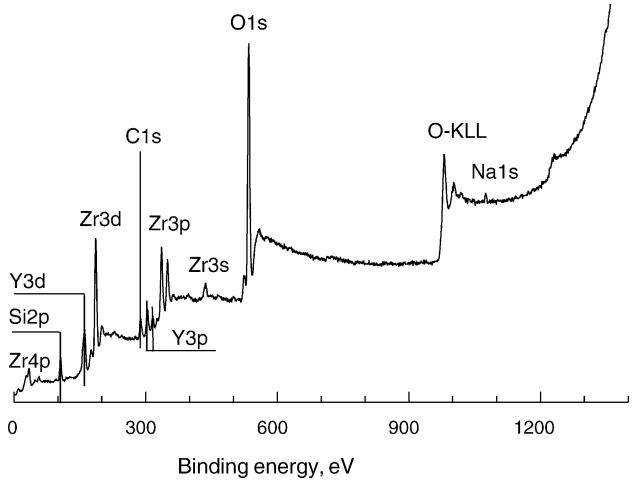

Fig. 4. Survey XPS spectrum of the 9Y-PSZ (five cycles) coated Nicalon^{TM} fiber.

Fig. 5 shows the O 1s, Y 3d and Zr 3d photopeaks. Deconvolution of the O 1s spectrum gives two components at 530.6 and 532.8 eV. Earlier Boronin et al.[16] studied a XPS spectrum of the Y-stabilized ZrO_2 single crystal in details. They detected a single O 1s peak at 530.6 eV which was assigned to oxygen in the metal–oxygen–metal bond, namely Y–O–Zr. One can propose that the low binding energy component that was observed in spectrum of Y-PSZ-coated Nicalon^{TM} fiber in this study also belongs to oxygen in the Y–O–Zr bond. Broadening of this peak (~2.7 eV) can be as evidence in favor of strong disordering of Y-doped zirconia phase. The second component at 532.8 eV in O 1s spectrum of Y-PSZ-coated Nicalon^{TM} fiber is only slightly shifted to lower binding energy in comparison with peak for uncoated Nicalon^{TM} fiber.[12] A slight shift to lower binding energy is observed also for Si 2p peak (Table 1). Analogous shifts O 1s and Si 2p lines in XPS spectrum of Y_2O_3 film on silicon was found by Chambers et al.[17] They detected also a shift of the Y $3d_{5/2}$ peak to higher binding energy (158.3 eV). On this basis they concluded that the formation of interfacial structure with the Y–O–Si bonds possible to occur. According to data listed in Table 1 and in Fig. 5b, the Y $3d_{5/2}$ peak for Y-PSZ-coated Nicalon^{TM} is in a good accordance with data by Moulder et al.[15] for pure Y_2O_3 and data reported by Zou et al.[18] Therefore, one could be reliably proposed that the formation of the Zr–O–Si, but not the Y–O–Si bonds is more expectable.

The XPS Zr $3d_{5/2}$ spectrum of Y-PSZ-coated Nicalon^{TM} fiber is shown in Fig. 5c. Deconvolution of this spectrum results in detection of two spin-orbital doublets. The position of one of them is in a good accordance with that reported for the YSZ single crystal.[16] Moreover, a strong broadening of peaks is observed. It can be connected with disordering of the oxide structure due to yttrium doping.[19,20] Actually, from the SEM analysis results it follows that the oxide coating is strongly nonuniform one and its integrity is disturbed (Fig. 3). An additional doublet appears to be an evidence of presence of zirconium bonded with SiO_2 surface layer of Nicalon^{TM} fiber.

3.3. XRD and Raman studies

The XRD patterns of the 3Y- (three cycles) and 9Y-PSZ (five cycles) coated Nicalon^{TM} fiber are represented in Fig. 6. Very small intensity peaks are present in XRD pattern of sam-

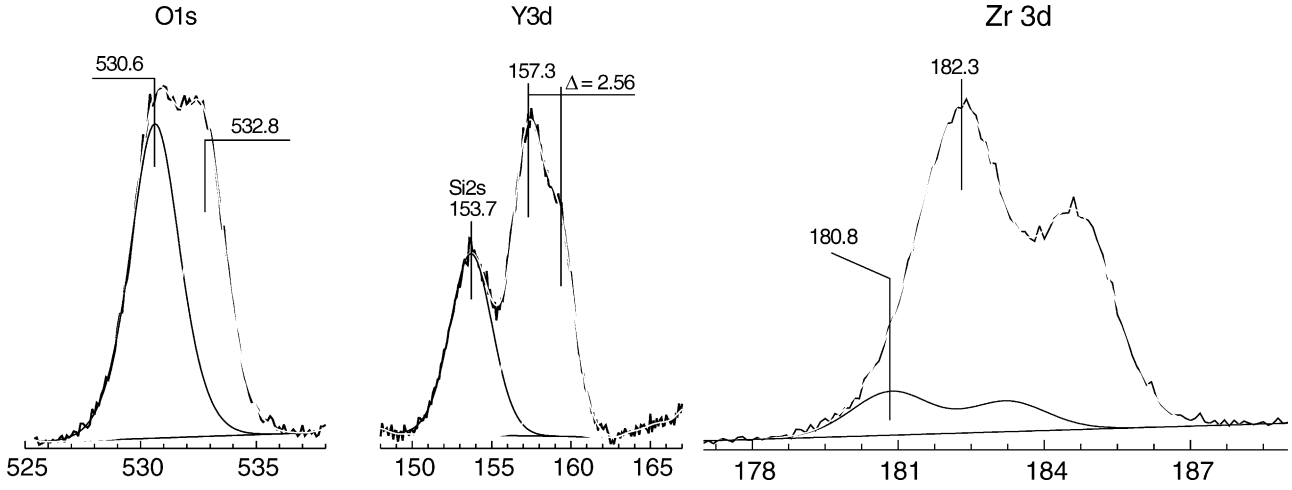

Fig. 5. XPS spectra of the 9Y-ZrO_2 (four cycles) coating on Nicalon^{TM} fiber: O 1s, Y 3d (c) and Z 3d photopeaks.

Table 1
Elemental composition and binding energies for the 9Y-ZrO_2-coated Nicalon^{TM} fibers

	O	Si	C	Zr	Y	Na
Elemental composition (at.%)	63	12.4	10	10	3.6	1
Binding energies (eV)	530.6, 532.8 (O 1s)	102.5 (Si 2p) 153.7 (Si 2s)	281.0, 284.8, 289.6 (C 1s)	182.3 (Zr 3 d5/2)	182.3 (Y 3d5/2)	1072.7 (Na 1s)

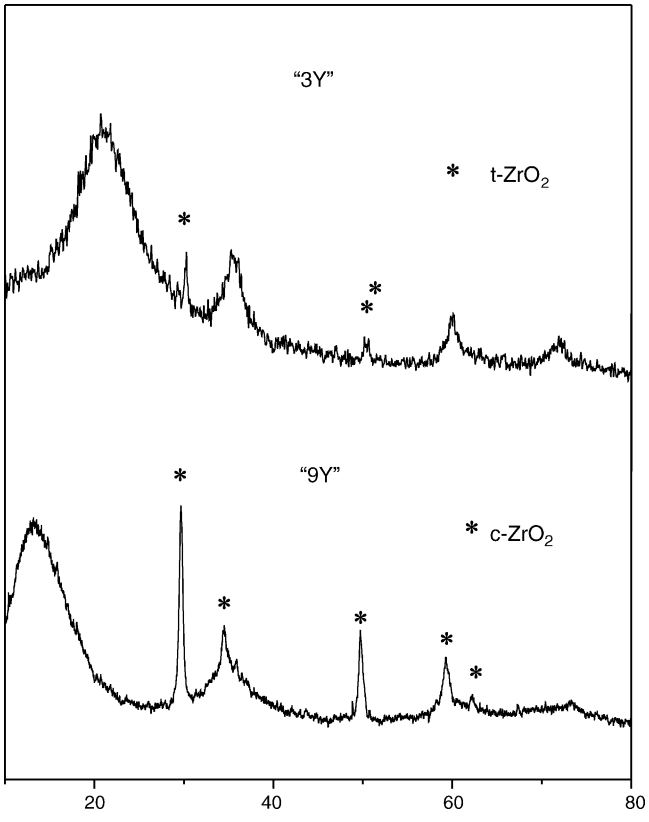

Fig. 6. The XRD patterns of the 3Y- and 9Y-PSZ-coated Nicalon™ fibers.

ple "3Y". They can be assigned to tetragonal zirconia phase (ICSD no. 42-1164). Sample "9Y" is cubic as expected. The XRD pattern coincides with that reported for fluorite-type structure (ICSD no. 27-0997). No traces of other zirconia phases are detected by X-ray analysis. Besides the ZrO_2 peaks, very broad features belonging to β-SiC phase of fiber are also observed in both XRD patterns.

For better interpretation of Raman results the spectra of Y-PSZ powders derived from the coatings precursors were taken preliminarily. Raman spectra of powders are represented in Fig. 7. For comparison a Raman spectrum of 0.5 mol% sol–gel derived zirconia powder is also shown. Clear changes in the main features of Raman spectra were observed for powders of various compositions. As one can see, in spectrum of 0.5Y-ZrO_2 at least 13 well-defined narrow bands are detected in the 100–800 cm^{-1} region (Fig. 7a). In accordance with data reported by Lopez et al.,[21] all of these bands can be assigned to monoclinic modification. Hardly noticeable feature to be comparable to noise can be detected at about 260 cm^{-1}. It is probably attributable to the strongest band of the tetragonal zirconia impurity.

Spectrum of the 3Y-ZrO_2 is sharply distinct from that of 0.5Y-ZrO_2 (Fig. 7b). It clearly shows six peaks at 148, 261, 320, 466, 609 (shoulder) and 641 cm^{-1}. Their number and positions are in a good coincidence with data reported by Lopez et al.[21] for tetragonal modification. So we can associate them with Raman active fundamentals for t-ZrO_2 and propose that the 3Y-ZrO_2 powder specimen is composed of

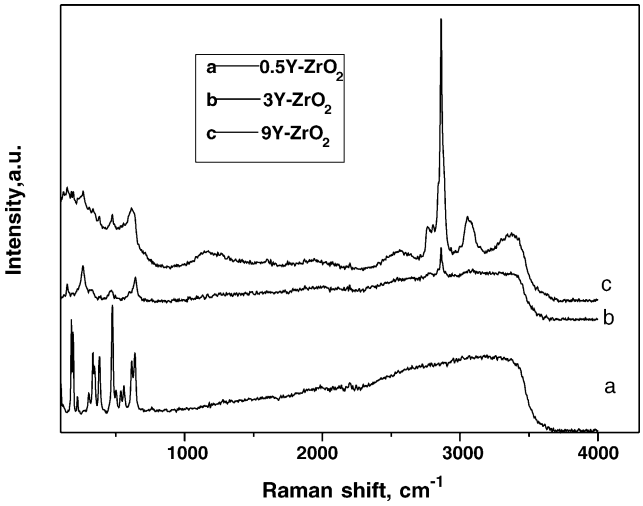

Fig. 7. Raman spectra (λ = 1064 nm) of 1Y-, 3Y-, and 9Y-doped ZrO_2 powders.

tetragonal modification only. The other important peculiarity of Raman spectrum of 3Y-ZrO_2 is in the fact that all of fundamentals are broadening. It can be assigned to structural disordering associated with oxygen vacancies in Y-doped samples. Additional features can be detected in the 1000–3500 cm^{-1} region, namely, small intensity bands at about 1000–1300 cm^{-1} and 1600 cm^{-1} and very intensive and narrow band at 2860 cm^{-1} together with new features at about 2770, 3058 and 3400 cm^{-1}.

The increase of yttria content in precursor up to 9 mol% results in the following change in Raman spectra of the 9Y-ZrO_2 powder (Fig. 7c). A major peak at 614 cm^{-1} is observed, the width being about 150 cm^{-1}. This is an evidence of the presence of cubic ZrO_2 modification. The width of this peak is anomalous owing to structural disordering in the oxygen sublattice. Interestingly, the Raman spectrum shows a peak at ∼260 cm^{-1} which can be attributed to tetragonal modification not detected by XRD (Fig. 6). The same additional features as in the 3Y-ZrO_2 spectrum are seen in the 1000–3500 cm^{-1} region, namely, very intensive and narrow peak at about 2870 and less intensive 2780 (shoulder), 2580 and 3067 cm^{-1} peaks.

Micro Raman spectra of 3Y- (three cycles) and 9Y-PSZ-coated (four cycles) Nicalon™ fiber (488 nm excitation wavelength) are represented in Fig. 8. All features in Raman spectrum of 3Y-PSZ-coated Nicalon™ fiber can be assigned to t-ZrO_2. As one can see from Fig. 8 (spectrum 9Y), the very broad and asymmetric peak at about 610 cm^{-1} is present together with several additional peaks. This behavior is attributed to disorder in the system due to ionic defects in the oxygen sublattice induced by acceptor. High defect concentration can lead to a breakdown of the selection rules and allow the additional modes that are forbidden for fluorite structure.[22] According to Raman data, the main component of coating is cubic ZrO_2 modification. The affinity of the positions of the rest peaks to those to be attributable to tetragonal

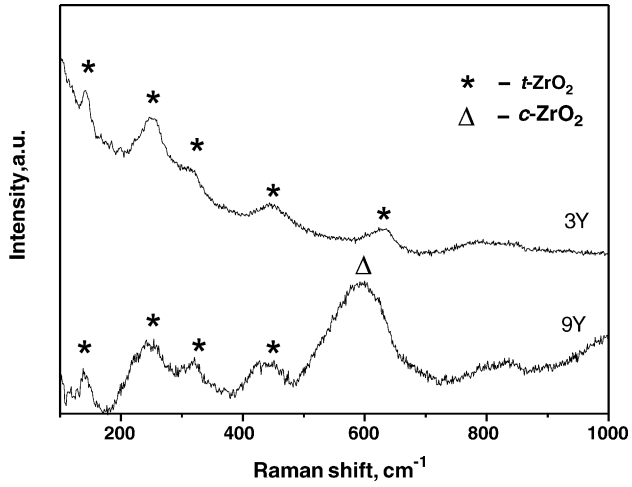

Fig. 8. Micro Raman spectra (λ = 488 nm) of the 3Y- and 9Y-PSZ-coated Nicalon™ fiber.

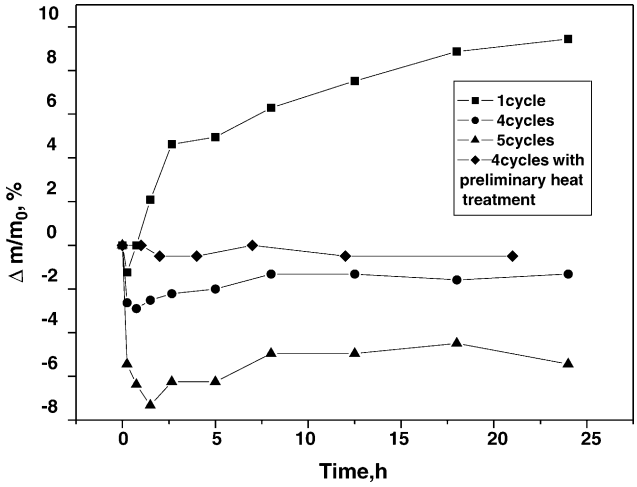

Fig. 9. Dependences of the relative mass $\Delta m/m_0$ on time at 1000 °C for the 9Y-doped ZrO_2-coated Nicalon™ fibers.

modification suggests the presence of t-ZrO_2 modification in coating layer too. The difference of Raman spectra of both coatings from those of powders derived from the same sols is in an absence any peaks in the 1000–3500 cm^{-1} region.

Summing up, one can state three groups of results to be discussed. The first group is concerned in the difference in Raman spectra in dependence on yttria content. With increasing of yttria content, the formation of monoclinic (0.5 mol% yttria), tetragonal (3%) and cubic (9%) modifications for sol-derived powders and coatings are clearly detected by Raman spectroscopy. Raman spectra of this study are in good accordance with those reported elsewhere for different zirconia modifications.

Further, the appearance of additional features in the 1000–1600 cm^{-1} and 2500–3500 cm^{-1} are observed for yttria-doped samples. As was noted by Strekalovsky et al.,[23] the peaks in the 1000–1300 cm^{-1} region can be assigned to the bending vibration of Me–O–H grouping (Me—Zr, Y). Taking into attention that this peak is observed only for 3Y- and 9Y-doped samples one can propose that the structures of gel particles of ZrO_2 with high (3Y and 9) and low (0.5Y) dopant level are different from each other. A greater number of water molecules bonding to terminal hydroxyl groups of Y-doped zirconia particles in comparison with low level doped appear to be retained between adjacent particles till up to 1000 °C. The appearance of small intensity ~1600 cm^{-1} (H_2O bending) and ~3050–3400 cm^{-1} (H_2O stretching) peaks in Raman spectrum can be as evidence in favor of this proposition.[24,25]

The group of very intensive and narrow peaks in the 2500–3100 cm^{-1} region is a subject of special consideration. The fact that these peaks are observable only in spectra taken using the 1064 nm and are absent in spectra taken using the 488 nm excitation wavelength suggests that the nature of these features is distinct from Raman scattering. Djurado et al.[26] and ref. 17 therein also mentioned the presence of intense peaks between 1000 and 1400 cm^{-1} in Raman spectrum ($\lambda_0 = 514.5$ nm) of nanocrystalline zirconia, whereas these peaks in Raman spectrum taken at $\lambda_0 = 488$ nm were absent. They unambiguously attributed these features to fluorescence peaks due to presumably defects resulting from

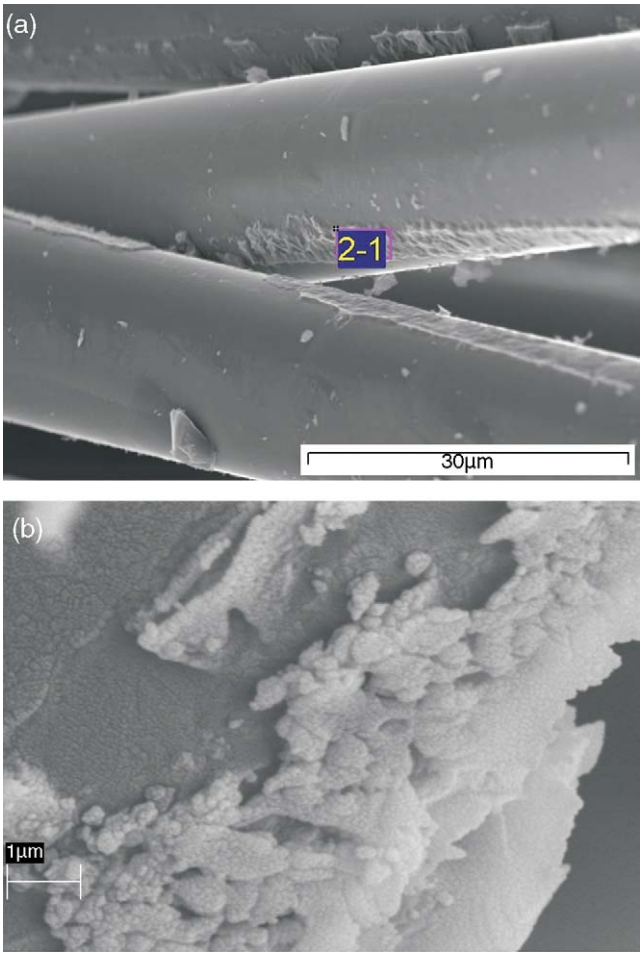

Fig. 10. SEM images of the surface of the 9Y-ZrO_2-coated Nicalon™ fibers (two cycles) after exposition to air at 1000 °C for 30 h (b: clear-up image).

initial preparation. It is well-known that doping of zirconium oxide by yttrium leads to the formation of defects, namely, oxygen vacancies. So one could be discreetly proposed that the peaks detected in Raman spectrum of Y-doped zirconia in the 2500–3000 cm^{-1} region could be attributed to fluorescence phenomenon. In any case, this phenomenon deserves to be more carefully and precisely studied in future.

3.4. Oxidation tests

Dependences of the relative mass $\Delta m/m_0$ on time at 1000 °C for 9Y-doped ZrO_2-coated Nicalon™ fibers (one, four and five cycles) are represented in Fig. 9. One can see, that the Y-doped ZrO_2-coated samples exhibit a similar overall behavior during oxidation test, namely: (i) first a sharp weight loss and (ii) a more progressive weight increase up to the test completion. The time corresponding to the transition between regimes (i) and (ii) is dependent on number of dipping-annealing cycles. For the 9Y-doped ZrO_2 (one cycle) sample this transition is detected approximately 1 h after the beginning of oxidation whereas for the 9Y-doped ZrO_2 (five cycles) the transition takes place later. As the number of dipping-annealing cycle during preparation of samples is increased the mass loss at the beginning of the oxidation becomes more pronounced. Beyond transition time the general trend in the $\Delta m/m_0$–t dependence is a weight increase but with a much lower rate.

Preliminary heat treatment of the Y-PSZ-coated Nicalon™ fibers for 3 h at 1000 °C in vacuum 0.1 Pa before oxidation testing leads to an insignificant mass loss (e.g. ~2.5% wt. for 9Y-ZrO_2, four dipping–annealing cycles). The following exposure of samples to air at 1000 °C leads to significant decrease in oxidation rate. As one can see from Fig. 9, an increase in number of dipping-annealing cycle (in different terms, the thickness of coating) gives rise to more oxidation resistant coated fibers.

3.5. SEM/EDS, X-ray and micro Raman analysis of oxidized coated fibers

SEM images of the surface of 9Y-ZrO_2-coated Nicalon™ fibers (two cycles) after exposition to air at 1000 °C for 30 h are represented in Fig. 10. The surface of oxidized filaments is not strongly distinguished from nonoxidized one. It is nonuniform and new formations of well-faceted shape and macro defects as traces from sol which was retained between separate monofilaments can be seen. The coating retains its integrity and no spalling is observed. It is seen from clear-up image of the surface of oxidized coated Nicalon™ fiber (Fig. 10b) that it is composed of isometric crystals in despite of the columnar microstructure that was early observed by Baklanova and coworkers[27] for oxidized undoped ZrO_2-coated Nicalon™ fiber. The elemental microanalysis by SEM/EDS

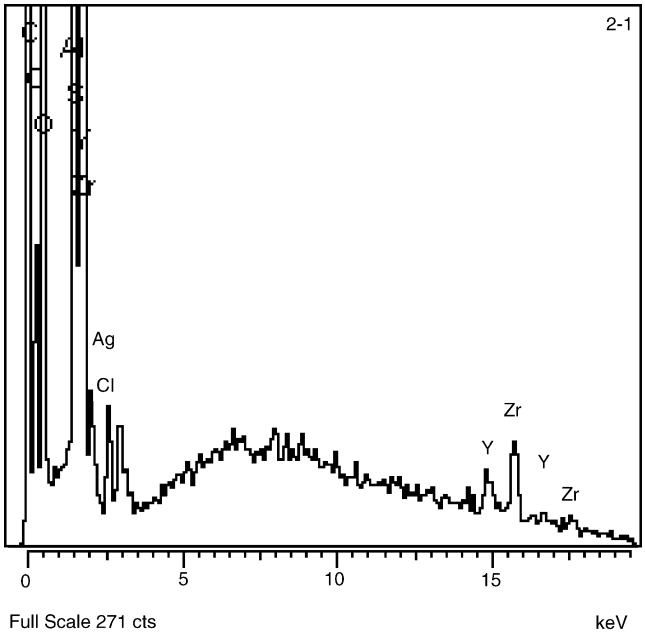

Fig. 11. EDS spectrum of the surface of the oxidized 9Y-ZrO_2 (two cycles) coating on Nicalon™ fiber.

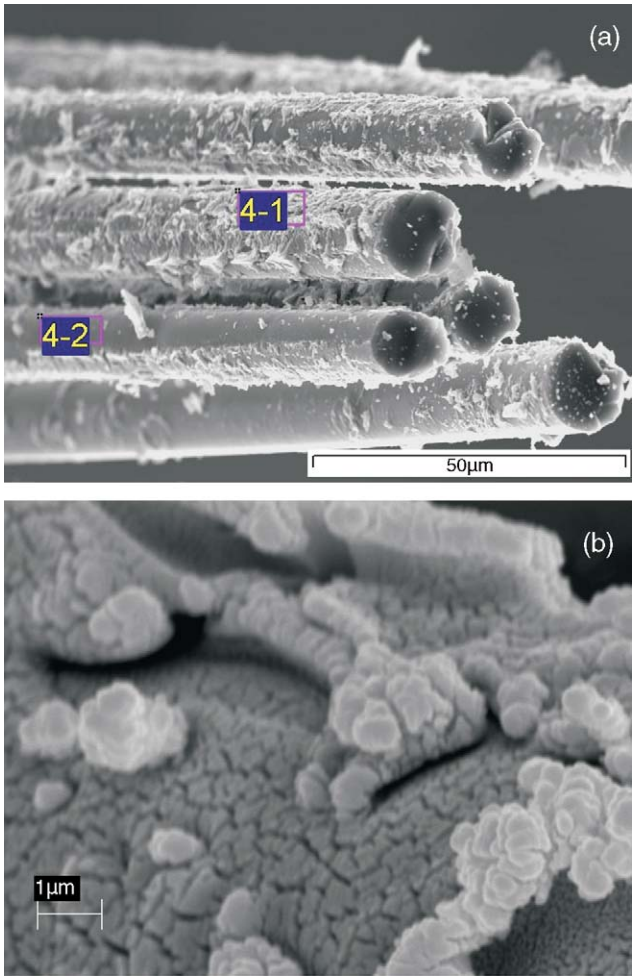

Fig. 12. SEM images of the 9Y-ZrO_2-coated Nicalon™ fibers (five cycles) after exposition to air at 1000 °C for 30 h.

of oxidized 9Y-ZrO_2 coating taken from different areas indicates the presence of Si, Zr, Y, Al (Fig. 11, see corresponding areas in Fig. 10a). The appearance of Al probably to be connected with a contamination from crucibles which were used for oxidation tests.

The oxidized Y-doped ZrO_2 coatings (five cycles) show a nonuniformity in greater extent in comparison with of coatings which were prepared using two dipping–annealing cycles (Fig. 12a and b). They exhibit an increased nonuniformity along length and diameter of monofilament. The other peculiarity is a presence of a great number of agglomerates composed from large crystals. The elemental analysis by SEM/EDS of oxidized 9Y-ZrO_2 coating (five cycles) taken from 1 and 2 areas (specified on Fig. 12a) indicates the presence of Si, Zr, Y as main constituents and Al as contamination (Fig. 13a and b). According to XRD data, at least c-ZrO_2 and crystobalite phases are present after exposition of coated fiber in air at 1000 °C for 30 h. Raman spectroscopy revealed c-ZrO_2 and possibly the tetragonal modification in coated fibers after oxidation.

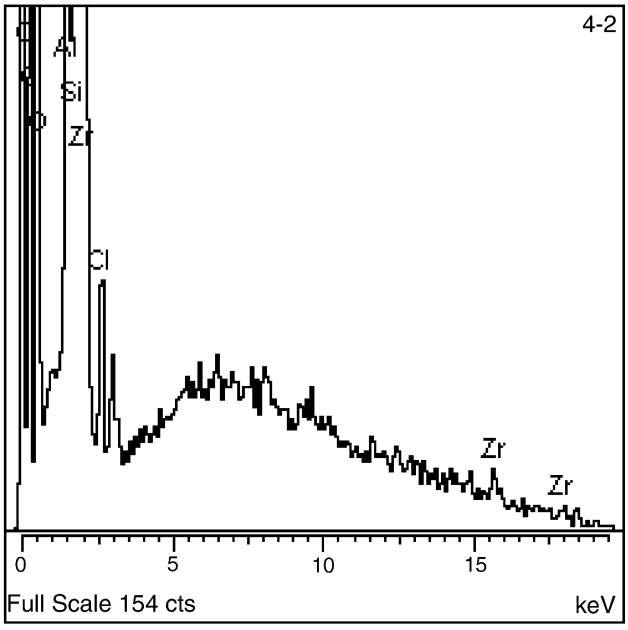

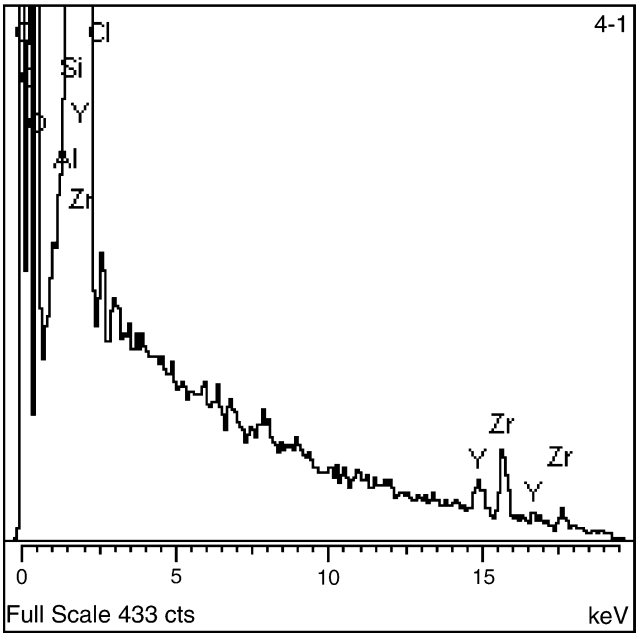

Fig. 13.

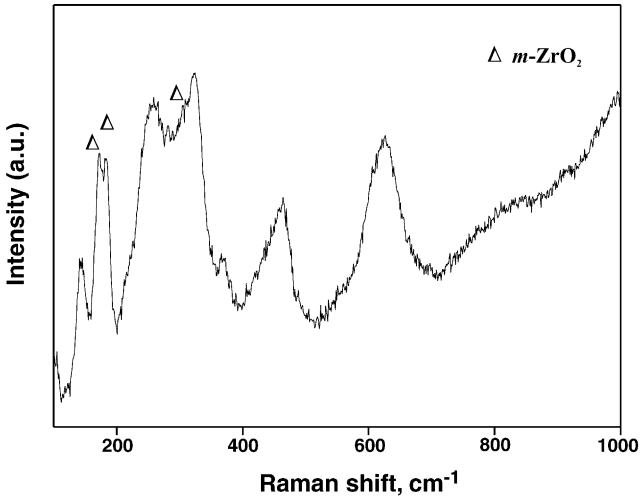

Fig. 14.

Raman spectra taken from separate areas of the oxidized 3Y-PSZ-coated fibers clearly demonstrate the presence of peaks belonging to t-ZrO_2 together with intensive peaks of monoclinic ZrO_2 modification (Fig. 14). One can note that no peaks other than belonging to tetragonal ZrO_2 modification were detected in Raman spectrum for nonoxidized specimen (see Fig. 8, 3Y).

4. Discussion

The opportunity for fabrication of the Y-doped zirconia interfacial coatings on Nicalon^{TM} fibers using sol–gel approach was clearly demonstrated in this study. In dependence of the yttrium dopant level the c- or t-ZrO_2 coatings on Nicalon^{TM} fiber were obtained using a simple way. However, in course of this study some peculiarities of interface chemistry, coating morphology and behavior in air at elevated temperatures of sol–gel derived Y-PSZ coatings on Nicalon^{TM} fibers were revealed and they must be discussed first of all.

As was mentioned above, the XRD and Raman analysis of 3Y-doped zirconia-coated Nicalon^{TM} fiber showed that the t-ZrO_2 is a main crystal phase of this coating. As to the 9Y-doped zirconia-coated Nicalon^{TM} fiber, the XRD patterns show peaks which are characteristic features of cubic ZrO_2 crystal phase. An analysis of Raman spectra of 9Y-doped-coated fibers and powders derived from the same precursors confirm that the cubic phase is a main component. How-

ever, as one can see from Figs. 7 and 8, the main peak at about 614 cm^{-1} is very broad and asymmetric one. Besides, in Raman spectra of both coatings and powders the additional features in the 100–1000 cm^{-1} are registered. Earlier it was reported that widening and asymmetry of main peak and the appearance of additional peaks in Raman spectrum of cubic ZrO_2 phase can be attributed to disorder in the system due to the oxygen vacancies induced by Y^{3+} acceptor.[21–23] High defect concentration in the oxygen sublattice can lead to a breakdown of the selection rules and allow the additional modes. As was mentioned above, the appearance of low binding energy O 1s photopeak at 530.6 eV in the XPS spectrum of Y-PSZ-coated Nicalon^{TM} fiber indicates to presence of the Y–O–Zr bonds in coating structure and large width of this peak to a strong disordering structure. Thus, taking into consideration of the XRD, XPS and Raman results, one can conclude that the composition of the 9Y-doped ZrO_2 interfacial coating on Nicalon^{TM} fiber is represented by strongly disordered cubic zirconia phase induced by Y^{3+} doping.

One can note the affinity of the positions of the rest Raman peaks observable in spectra of 9Y-doped zirconia-coated Nicalon^{TM} fibers to those reported for tetragonal modification.[21,23] It suggests that the t-ZrO_2 modification possible to be present too in despite of the fact that the tetragonal zirconia impurities were not detected by XRD. As was noted by many authors (see, e.g.[21]), Raman spectroscopy seems to be more sensitive than XRD in detecting of these impurities. Thus, taking into consideration of the XRD, XPS and Raman results, one can conclude that the composition of the 3Y-doped ZrO_2 interfacial coating on Nicalon^{TM} fiber is represented only by tetragonal crystal phase, whereas the 9Y-doped ZrO_2 interfacial coating on Nicalon^{TM} fiber is represented mainly by strongly disordered cubic zirconia phase of induced by Y^{3+} doping and tetragonal modification as an impurity. It should be emphasized that the question concerning an accurate control of phase composition of ZrO_2-based coating is of great interest because it is well-established that the zirconia crystal phases are strongly differ from each other by their ability to "low-temperature" degradation[28 and refs. therein] and a tough transformation.[10]

Another reason resulting in more complex composition of coating is a possible interaction of Y-doped zirconia coating with support during processing and operating. The XPS results obtained in this study showed that the Zr–O–Si bonds appear to be formed at the fiber-coating interface region. Actually, according to Jarvis and Carter,[29] adhesion energy at the ZrO_2/SiO_2 interface is quite high and a very strong bonding and a dramatic rearrangement of the atomic coordinates exist at this interface. They concluded that chemical bonding provides a significant source of interface strengthening even at ambient temperature and in the absence of a new reaction phase. Earlier, White and coworkers[30] examined the ZrO_2/SiO_2 interfacial zone of thin ZrO_2 films on silicon using XPS and presumed that the formation of $ZrSiO_4$ occurs. As to the formation of the Y–O–Si bonds, it is questionable taking into consideration of the XPS results of this study. Further careful investigation must be carried out to clarify this question.

According to Raman spectroscopy results, a small quantity of residual OH-groupings and H_2O molecules can be present in as-received Y-PSZ coating structure and contribute to disordering of coating structure. Besides, the traces of nitrogen atoms (derived from the initial yttrium nitrate) in coating was determined by the XPS analysis. Although chlorine atoms were not detected by XPS, nevertheless the presence of residual chloride ions in as-received coating must not be excluded too. Owing to preliminary heat treatment of coated Nicalon^{TM} fiber at 600 °C in vacuum 10^{-6} Pa before the XPS measurements, the gaseous chlorine-containing compounds could be escaped and as result not be detected by XPS analysis. Thus, as was stated in this study, the sol–gel derived Y-doped ZrO_2-based coatings are characterized by a complex elemental and crystal phase composition. This circumstance must be taken into consideration on examination of the oxidation test results. Actually, as was shown in this study, preliminary heat treatment in vacuum of the as-received Y-PSZ-coated fibers with following exposure to air at 1000 °C results in a significant decrease of the oxidation rate. During preliminary annealing a removal of residual groupings derived from sol precursors, an ordering of the coating structure and an improvement of the coating texture appear to occur. As a result, higher quality coatings with improved oxidation resistance are formed.

The other question to be discussed is a weak interface behavior of Y-PSZ coating on Nicalon^{TM} fiber that was demonstrated in this study and a possible role of ZrO_2 phase transformations on this behavior. As was shown in this study, a controlled addition of yttria to zirconia results in the formation of ZrO_2-based coating, consisting of metastable tetragonal phase or metastable tetragonal phase in the cubic "matrix". If a stress due to some cracks is applied to the metastable tetragonal particles, a stress induced phase transition from metastable tetragonal to the stable monoclinic phase occurs. As the phase transformation is accompanied by large volume dilation and shear, further growth of crack is suppressed.[10] It should be noted that the c → t′ transformation also occurs with the volume dilation, the volume dilation being smaller than for the t → m transformation. If this transformations take place within interfacial zone a significant compressive stresses might cause the ZrO_2 coating to delaminate. Actually, a delamination phenomenon was observed within thick 9Y-PSZ (five cycles) coating on Nicalon^{TM} fiber (Fig. 3). As was mentioned above, in Raman spectra taken from some areas of oxidized 3Y-PSZ-coated fibers the peaks belonging to monoclinic modification and yttrium oxide as separate phase together with tetragonal modification were detected (Fig. 14), with neither m-ZrO_2, nor Y_2O_3 were detected in this coating before oxidation tests. This fact is a serious argument in favor of delamination induced by the t → m phase transformation. Nevertheless, a contribution of the CTE mismatch of Y-PSZ and SiO_2 phases must not

be excluded too. The more thorough investigation must be undertaken in future to clarify this controversial issue.

As was noted by Lee and coworkers,[8] not only the weak interface character but the integrity and uniformity of the fiber coating are important in terms of protecting the fiber surface from matrix infiltration by CVI or melt infiltration. From this point of view, a dense undelaminated but compressively stressed coating, e.g. based on the c- or t-ZrO_2 modification might be preferred before infiltration. Our results clearly demonstrate that an accurate ZrO_2 phase control and as a consequence, the extent of the phase transformations in the ZrO_2 coating for optimization interfacial properties can be readily attained using approach developed in this study.

5. Conclusion

Sols of yttria-stabilized zirconia were used as simple, readily processable and accurate controllable precursors for the ZrO_2 interfacial coatings on SiC-based Nicalon^{TM} fibers. It was shown that the ZrO_2 interfacial coatings of predictable compositions including transformable tetragonal and cubic crystal phases can be readily obtained in dependence of Y_2O_3 dopant level. The morphology, composition, structure and oxidation resistance of coated fibers were evaluated by SEM, EDS, XPS, XRD, and Raman analysis. All coatings obtained are uniform, continuous and adherent to substrates. For samples prepared using multiple dipping-annealing the coating consisted of large grained isometric crystals. The delamination within the ZrO_2 interfacial coating was observed. It was proposed that the t → m or c → t tough transformation of zirconia phase can be responsible for this phenomenon. The peculiarities of the behavior of Y-stabilized ZrO_2-coated fibers in air at elevated temperature are considered.

Acknowledgements

The authors are grateful to Mrs. T.M. Zima for supplying of m-ZrO_2 powder and Dr. B.A. Kolesov (Institute of Inorganic Chemistry SB RAS) for micro Raman measurements.

References

1. Kerans, R. J., Hay, R. S., Parthasarathy, T. A. and Cinibulk, M. K., Interface design for oxidation-resistant ceramic composites. *J. Am. Ceram. Soc.*, 2002, **85**(11), 2599–2632.
2. Filipuzzi, L., Camus, G., Naslain, R. and Thebault, J., Oxidation mechanism and kinetics of 1D-SiC/C/SiC composite materials. I: An experimental approach. *J. Am. Ceram. Soc.*, 1994, **77**(2), 459–466.
3. Sheldon, B. W., Sun, E. Y., Nutt, S. R. and Brennan, J. J., Oxidation of BN-coated SiC fibers in ceramic matrix composites. *J. Am. Ceram. Soc.*, 1996, **79**(2), 539–543.
4. Lee, W. Y., Lara-Curzio, E. and More, K. L., Multilayered oxide interphase concept for ceramic-matrix composites. *J. Am. Ceram. Soc.*, 1998, **81**(3), 717–720.
5. Zima, T. M., Baklanova, N. I., Belyaeva, E. I., Boronin, A. I. and Kosheev, S. V., Sol–gel derived coatings on Nicalon^{TM} fiber. *Ceram. Eng. Sci. Proc. A*, 2003, **24**(3), 463–468.
6. Verdenelli, M., Parola, S., Chassagneux, F., Letoffe, J.-M., Vincent, H., Scharff, J.-P. *et al.*, Sol–gel preparation and thermo-mechanical properties of porous xAl_2O_3–$ySiO_2$ coatings on SiC Hi-Nicalon fibres. *J. Eur. Ceram. Soc.*, 2003, **23**(8), 1207–1213.
7. Li, H., Lee, J. and Lee, W. Y., Effects of air leaks on the phase content, microstructure, and interfacial behavior of CVD zirconia on SiC fiber. *Ceram. Eng. Sci. Proc. B*, 2002, **23**(4), 261–268.
8. Li, H., Lee, J., Libera, M. R., Lee, W. Y., Kebbede, A., Lance, M. J. *et al.*, Morphological evolution and weak interface development within chemical-vapor-deposited zirconia coating deposited on Hi-Nicalon^{TM} fiber. *J. Am. Ceram. Soc.*, 2002, **85**(6), 1561–1568.
9. Lee, J., Li, H., Lee, W. Y. and Lance, M. J., Effects of oxygen partial pressure on the nucleation behavior and morphology of chemically-vapor-deposited zirconia on Hi-Nicalon fiber and Si. *J. Am. Ceram. Soc.*, 2003, **86**(12), 2031–2036.
10. Bocanegra-Bernal, M. H. and Diaz de la Torre, S., Review. Phase transformations in zirconium dioxide and related materials for high performance engineering ceramics. *J. Mater. Sci.*, 2002, **37**(23), 4947–4971.
11. Ruddel, D. E., Stoner, B. R. and Thompson, J. Y., The effect of deposition parameters on the properties of yttria-stabilized zirconia thin films. *Thin Solid Films*, 2003, **445**(1), 14–19.
12. Baklanova, N. I., Zima, T. M., Naimushina, T. M. and Kosheev, S. V., The formation of refractory oxide coatings on Nicalon^{TM} fiber by sol–gel process. *J. Eur. Ceram. Soc.*, 2004, **24**(10–11), 3139–3148.
13. Zhang, Y.-W., Yang, Y., Jin, S., Liao, C.-S. and Yan, C.-H., Long time annealing effects on the microstructures of the sol–gel-derived nanocrystalline thin films of rare earth-stabilized zirconia. *J. Mater. Chem.*, 2001, **11**(8), 2067–2071.
14. Zhang, Y.-W., Yang, Y., Tian, S. J., Liao, C.-S. and Yan, C.-H., Sol–gel synthesis and electrical properties of $(ZrO_2)0.85(REO_{1.5})0.15$ (RE = Sc, Y) solid solutions. *J. Mater. Chem.*, 2002, **12**(2), 219–224.
15. Moulder, J. F., Stickle, W. F., Sobol, P. E. and Bomben, K. D., *Handbook of X-Ray Photoelectron Spectroscopy*. Perkin-Elmer, Eden Prairie, MN, 1992.
16. Boronin, A. I., Kvon, R. I. and Sobyanin, V.A., Pd and Ag films on the surface of yttria stabilized zirconia monocrystal. In *Proceedings of the XI Conference on Physical Chemistry and Electrochemistry of Alloyed and Solid Electrolytes, Vol. VII*. Ekaterinburg, Russia, 1998, pp. 27–28 (in Russian).
17. Chambers, J. J., Busch, B. W., Gustafsson, T., Garfunkel, E., Wang, S., Maher, D. M. *et al.*, Effects of surface pretreatments on interface structure during formation of ultra-thin yttrium silicate dielectric films on silicon. *Appl. Surf. Sci.*, 2001, **181**(1–2), 78–93.
18. Zou, G., Fang, K., He, P. S. and Song, H. S., Preparation of Y_2O_3-stabilized ZrO_2 thin electrolyte films from Langmuir–Blodgett film precursors by means of "surface ions". *J. Mater. Chem.*, 2002, **12**(10), 2998–3002.
19. Michel, D., Perez, Y., Jorba, H. and Collongues, R., Etude de la transformation ordre desordre de la structure fluorite a la structure pyrochlore pour des phases $(1-x)ZrO_2$–xLa_2O_3. *Mater. Res. Bull.*, 1974, **9**(11), 1457.
20. Scheetz, B. E. and White, W. B., Characterization of anion disorder in zirconate $A_2B_2O_7$ compounds by Raman spectroscopy. *J. Am. Ceram. Soc.*, 1979, **62**(9–10), 468.
21. Lopez, E. F., Escribano, V. S., Panizza, M., Carnasciali, M. M. and Busca, G., Vibrational and electronic spectroscopic properties of zirconia powders. *J. Mater. Chem.*, 2001, **11**(7), 1891–1897.
22. Kosacki, I., Petrovsky, V. and Anderson, H. U., Raman spectroscopy of nanocrystalline ceria and zirconia thin films. *J. Am. Ceram. Soc.*, 2002, **85**(11), 2646–2650.

23. Strekalovsky, V. N., Makurin, Yu. N. and Vovkotrub, E. G., Study of phase transformation and defects in the ZrO_2–Y_2O_3 system by Raman spectroscopy. *Inorg. Mater.*, 1983, **19**(6), 925–929 (in Russian).
24. Nakamoto, K., *Infrared Spectra and Raman Spectra of Inorganic and Coordination Compounds*. John Wiley and Sons, New York, 1991, p. 120.
25. Yukhnevich, G. V., Infrared spectroscopy of water. *Science Moscow*, 1973, 111–114 (in Russian).
26. Djurado, E., Bouvier, P. and Lucazeau, G., Crystallite size effect on the tetragonal–monoclinic transition of undoped nanocrystalline zirconia studied by XRD and Raman Spectroscopy. *J. Solid State Chem.*, 2000, **149**(2), 399–407.
27. Zima, T. M., Baklanova, N. I. and Titov, A.T., The behavior of the oxide coated Nicalon^{TM} fibers exposed to air at 1000 °C. *J. Eur. Ceram. Soc.*, in press.
28. Guo, X., On the degradation of zirconia ceramics during low-temperature annealing in water or water vapor. *J. Phys. Chem. Solids*, 1999, **60**(4), 539–546.
29. Jarvis, E. A. A. and Carter, E. A., Exploiting covalency to enhance metal–oxide and oxide– oxide adhesion at heterogeneous interfaces. *J. Am. Ceram. Soc.*, 2003, **86**(3), 373–386.
30. Sun, Y. M., Lozano, J., Ho, H., Park, H. J., Veldman, S. and White, J. M., Interfacial silicon oxide formation during synthesis of ZrO_2 on Si(1 0 0). *Appl. Surf. Sci.*, 2000, **161**(2), 115–122.